Cancer Letters 469 (2020) 355–366

Contents lists available at ScienceDirect

Cancer Letters

journal homepage: www.elsevier.com/locate/canlet

Original Articles

PD-L1$^+$ aneuploid circulating tumor endothelial cells (CTECs) exhibit resistance to the checkpoint blockade immunotherapy in advanced NSCLC patients

Lina Zhang[a,1], Xinyong Zhang[b,1], Yanxia Liu[a,b], Tongmei Zhang[b], Ziyu Wang[a], Meng Gu[a], Yilin Li[c], Daisy Dandan Wang[d], Weiying Li[a,**], Peter Ping Lin[d,*]

[a] Department of Cellular and Molecular Biology, Beijing Chest Hospital, Capital Medical University, Beijing Tuberculosis and Thoracic Tumor Research Institute, Beijing, China
[b] Department of Medical Oncology, Beijing Chest Hospital, Capital Medical University, Beijing Tuberculosis and Thoracic Tumor Research Institute, Beijing, China
[c] Key Laboratory of Carcinogenesis and Translational Research (Ministry of Education), Department of GI Oncology, Peking University Cancer Hospital & Institute, Beijing, China
[d] Cytelligen, San Diego, CA, USA

ARTICLE INFO

Keywords:
Aneuploid CTC and CTEC
Post-therapeutic karyotype shifting
Cellular circulating tumor biomarker
Liquid biopsy
SE-iFISH

ABSTRACT

Sustained angiogenesis and increased PD-L1 expression on endothelial and carcinoma cells contribute toward fostering an immunosuppressive microenvironment suitable for tumor growth. PD-L1$^+$ CTCs were reported to associate with poor prognosis in NSCLC patients. However, whether or not aneuploid circulating tumor endothelial cells (CTECs) express PD-L1, then serve as a surrogate biomarker to evaluate immunotherapy efficacy remains unknown. In this study, a novel SE-iFISH strategy was established to comprehensively quantify and characterize a full spectrum of aneuploid CTCs and CTECs in advanced NSCLC patients subjected to second-line anti-PD-1 (nivolumab) immunotherapy. *In situ* co-detection of diverse subtypes of aneuploid CTCs and CTECs expressing PD-L1 and Vimentin was performed. The present clinical study demonstrated that significant amounts of PD-L1$^+$ aneuploid CTCs and CTECs could be detected in histopathologic hPD-L1$^-$ patients. In contrast to decreased PD-L1$^+$ CTCs, the number of multiploid PD-L1$^+$ CTECs (≥tetrasomy 8) undergoing post-therapeutic karyotype shifting increased in patients along with tumor progression following anti-PD-1 treatment. Progressive disease (PD) lung cancer patients possessing multiploid PD-L1$^+$ CTECs had a significantly shorter PFS compared to those without PD-L1$^+$ CTECs. In carcinoma patients, aneuploid CTCs and CTECs may exhibit a functional interplay with respect to tumor angiogenesis, progression, metastasis, and response to immunotherapy.

1. Introduction

Aberrant immune cells, sustained angiogenesis, dysfunctional angiogenic vasculatures in solid tumors, and increased PD-L1 expression on endothelial as well as neoplastic cells, all contribute toward constituting an immunosuppressive microenvironment suitable for tumor growth. In the primary lesion, where tumor cells and the host's immune system interact, a microenvironment favorable for cancer development and metastasis is fostered [1]. It has been illustrated that the tumor microenvironment is mainly constituted by proliferating tumor cells, infiltrating inflammatory cells, blood vessels, stroma cells and surrounding tissue cells. Among the tumor infiltrating inflammatory lymphocytes, T cells are the major component [2].

Cytotoxic T-lymphocyte-associate protein 4 (CTLA-4, CD152), CD80 (B7-1), and programmed cell death 1 protein (PD-1, CD279), known as immune checkpoints, are inhibitory receptors expressed on diverse T cell subpopulations [3,4]. Those immune checkpoint receptors interact with their relevant ligands in the tumor microenvironment, and subsequently down-regulate T cell activation and cytolytic activity of tumor-infiltrating CD4$^+$/CD8$^+$ T cells in response to inflammatory stimuli, thus rendering malignant cancer cells the ability to resist and evade immune attack [5]. Ligands for PD-1 receptor and CD80 are programmed death-ligand 1 (PD-L1, CD274, B7–H1) and PD-L2 (CD273, B7-DC). PD-L1 is the primary ligand for PD-1, and is

* Corresponding author.
** Corresponding author.
E-mail addresses: li_weiying412@aliyun.com (W. Li), plin@cytelligen.com (P.P. Lin).
[1] These authors contributed equally to this work.

https://doi.org/10.1016/j.canlet.2019.10.041
Received 25 July 2019; Received in revised form 22 October 2019; Accepted 27 October 2019

Abbreviations

ap	aneuploid
TEC	tumor endothelial cell
CTEC	circulating tumor endothelial cell
CTC	circulating tumor cell
sCTC/CTEC	small CTC/CTEC
$_{L}$CTC/CTEC	large CTC/CTEC
EMT	epithelial-to-mesenchymal transition
EndoMT	endothelial-to-mesenchymal transition
hPD-L1	histopathological PD-L1 expression
PD	progressive disease
iFISH	immunostaining-fluorescence *in situ* hybridization

overexpressed on a series of solid tumor cells, endothelial cells [6], and other cells in the tumor microenvironment [7].

A great endeavor of cancer immunotherapies, which effectively interrupt and inhibit the binding of immune checkpoint receptors to their ligands, have been shown to enhance T cell response to malignant carcinoma cells in the tumor microenvironment. USFDA approved immune checkpoint inhibitors, including immunotherapeutic monoclonal antibodies against checkpoint receptors such as PD-1 (Keytruda pembrolizumab by Merck; Opdivo nivolumab by Bristol-Meyers Squibb), CTAL-4 (Yervoy ipilimumab by BMS), or against the ligand PD-L1 (Tecentriq atezolizumab by Roche; Imfinzi durvalumab by AstraZeneca; Bavencio avelumab by Merck and Pfizer), have demonstrated unique advantages in restoring and facilitating appropriate immune response, ultimately eliminating carcinoma cells [8].

It has been reported that among non-small cell lung cancer (NSCLC) patients subjected to anti-PD-1 checkpoint blockade immunotherapy, longer progression-free survival (PFS) and overall survival (OS) were observed in patients whose tumor cells highly expressed PD-L1 (tumor proportion score > 50%) [9]. Examination of PD-L1 expression on cancer cells is pivotal for guiding administration of anti-PD-1 to cancer patients. However, distribution of PD-L1$^+$ neoplastic cells in tumors is not homogeneous, as those cells are clustered in the specific region where IFNγ−activated T cells infiltrate rather than diffuse in tumor tissue [10]. Conventional histopathologic needle biopsy thus may bring a non-negligible false negative hPD-L1 detection [4]. Moreover, similar to the conventional detection of histopathologic hHER2 expression, invasive needle biopsy, routinely performed only once, is evidently not suitable for dynamically monitoring the expression of HER2 or PD-L1on cancer cells. Recent progress in non-invasive liquid biopsy has made it feasible to periodically or constantly monitor dynamic expression of PD-L1 or HER2 on circulating tumor cells (CTCs) [11], which could serve as a surrogate marker available for frequent detections in cancer patients.

CTCs, cancer cells that are shed from primary or metastatic solid tumors into peripheral blood, are relevant to tumor metastasis and progression [12–14]. Aneuploid CD31$^+$ circulating tumor endothelial cells (CTECs) [15,16], are derived from CD31$^+$ aneuploid tumor endothelial cells (TECs) in tumor tissue [17,18]. The clinical significance of TECs in cancer metastasis and progression [19,20], and CTECs' role in tumor angiogenesis have been substantially investigated [21,22]. Of particular interest is the substantial expression of a variety of tumor biomarkers and the stemness marker on CTECs that has been recently reported [23].

Expression of PD-L1 on both CTCs [24] and TECs [25,26] has been published elsewhere. Recent study indicated that high PD-L1 expression on carcinoma cells is associated with the Vimentin$^+$ mesenchymal phenotype in cancer cells [27]. Investigation of clinical utilities of PD-L1$^+$ CTCs and TECs [25] in various carcinoma patients has rapidly gained close attention in the field [28–32]. Whether or not PD-L1 is expressed on aneuploid CTECs and then serves as a surrogate biomarker to evaluate immunotherapy efficacy, however, remains unclear.

In the present study, following our previous demonstration of PD-L1 expression on aneuploid cancer cells and CTCs [16,33], a novel integrated strategy of subtraction enrichment and immunostaining-fluorescence *in situ* hybridization (SE-iFISH) [34], was further optimized to perform comprehensive *in situ* phenotypic, karyotypic and morphological characterized of a full spectrum of aneuploid circulating rare cells, including CTCs and particularly CTECs in advanced NSCLC patients treated with second-line anti-PD-1 (nivolumab). Expression of PD-L1 and the mesenchymal marker Vimentin (Vim) on aneuploid CTECs and CTCs was co-detected in lung cancer patients. PD-L1$^+$ CTECs, identified and characterize for the first time in the current study, were found to undergo both post-therapeutic karyotype and morphology shifting following immunotherapy. Although second-line anti-PD-1 could effectively deplete the specific subtype of haploid small cell size CTCs and CTECs (≤5 μm WBCs), the quantity of multiploid large PD-L1$^+$ CTECs (≥tetrasomy 8) significantly increased in immunotherapeutic patients. Post-therapeutic NSCLC progressive disease (PD) patients possessing the specific subtype of multiploid PD-L1$^+$ CTECs showed a significantly shorter PFS compared to those who had no PD-L1$^+$ CTEC detected, indicating that PD-L1$^+$ CTECs were associated with anti-PD-1 resistance and tumor progression.

Unlike small fragments of circulating tumor nucleic acids (ctDNA) that are diluted in peripheral circulation, both CTCs and tumor angiogenesis related CTECs constitute a category of viable, real time "cellular circulating tumor biomarkers", which contain intact contents of genomic and protein expression profiles or the signatures along with tumor progression. Each sub-category of those non-hematologic aneuploid circulating rare cells may distinctively possess diverse clinical utilities, and manifest a functional interplay with respect to facilitating tumor progression, circulation, seeding as well as implantation of metastatic cancer cells in carcinoma patients.

2. Materials and methods

2.1. Patients' enrollment and specimen collection

SE-iFISH was applied to comprehensively detect and characterize PD-L1$^+$ and Vimentin$^+$ aneuploid CTCs and CTECs. A total of 16 advanced NSCLC patients were enrolled. Fourteen patients failed first-line chemotherapy and received second-line anti-PD-1 nivolumab treatment. Remaining 2 patients were subjected to first-line nivolumab therapy.

Consent forms signed by all subjects were approved by the Ethics Review Committees (ERC) of Beijing Chest Hospital, Capital Medical University, Beijing, China. The written consent forms were received from each patient prior to blood collection. The clinical study was performed according to the Declaration of Helsinki Principles.

Six ml of peripheral blood were periodically collected from pre- and post-immunotherapeutic patients at the indicated time intervals, i.e. once in every 4 nivolumab treatment cycles until PD was developed. Some patients were unable to provide blood specimens as scheduled due to unforeseeable clinical complications. Samples of post-PD patients were not counted in this study due to subsequent change of therapy regimen.

2.2. Subtraction enrichment (SE)

Subtraction enrichment was performed according to the manufacture's updated instruction with minor modifications (Cytelligen, San Diego, CA, USA) [16], or using an automated i•Cyto® Biofluid Specimen Processor (Model: BSP-01A, Cytelligen). Briefly, 6 ml of blood were

collected into a tube containing ACD anti-coagulant (Becton Dickinson, Franklin Lakes, NJ, USA). Blood samples were centrifuged at 200 × *g* for 15 min at room temperature to separate plasma. Sedimented blood cells were mixed with 3.5 ml of hCTC buffer, followed by loading on the top of non-hematopoietic cell separation matrix in a 50 ml tube. Samples were subjected to centrifugation at 450 × *g* for 5 min. Solution containing WBCs and tumor cells above RBCs was collected into a 50 ml tube, and subsequently incubated with 300 μl of immuno-magnetic beads conjugated to a cocktail of anti-leukocyte mAbs at room temperature for 30 min. WBCs bound to immuno-beads were depleted using a 50 ml size magnetic separator (Cytelligen). The solution, free of magnetic beads, was collected into a 15 ml tube, followed by adding hCTC buffer to 14 ml. Samples were then spun at 500 × *g* for 4 min at room temperature, followed by aspirating supernatants down to 100 μl. Sedimented cells were gently resuspended and mixed with the cell fixative (Cytelligen). The cell mixture was smeared on the formatted and coated CTC slides, and dried for subsequent iFISH processing.

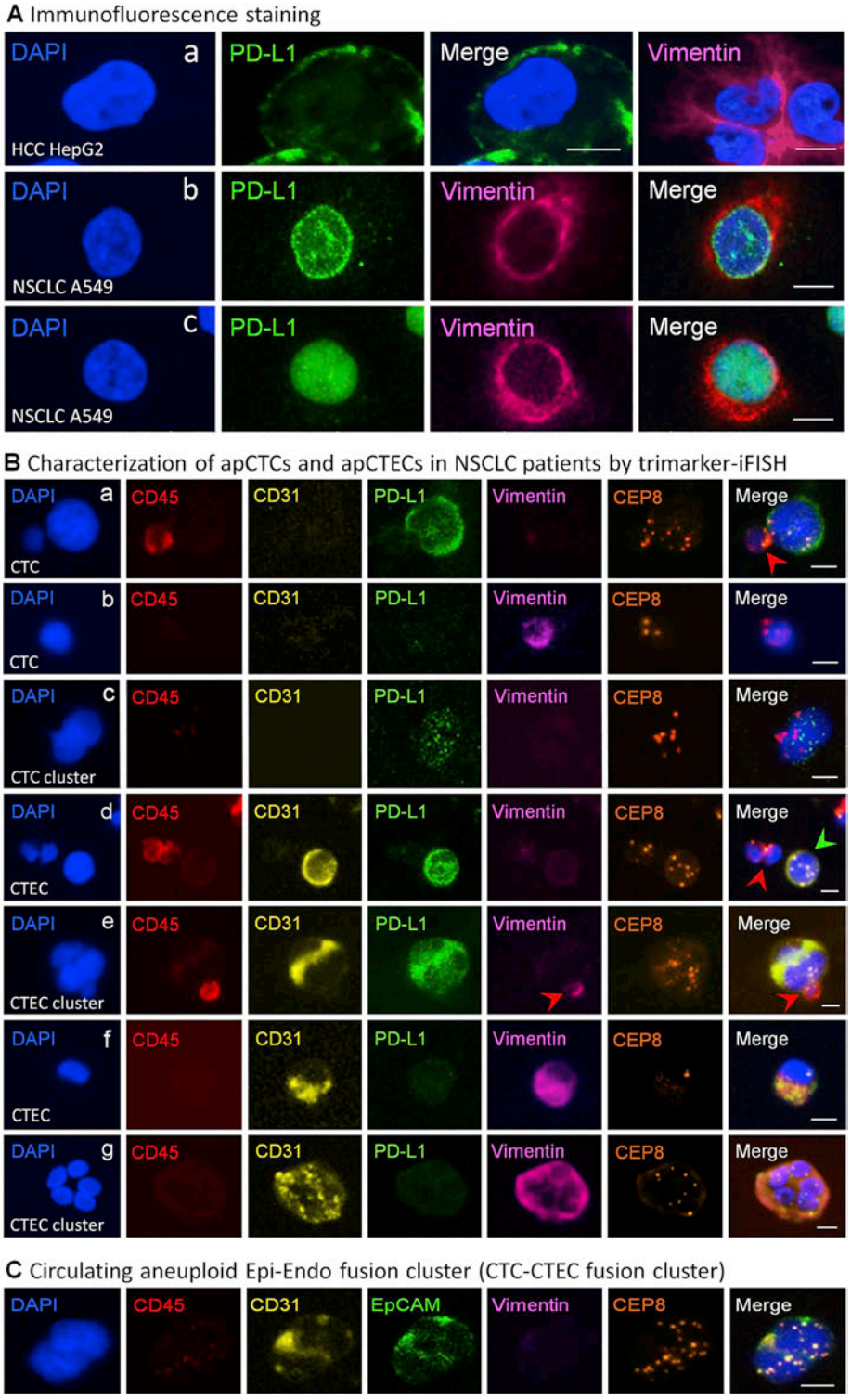

Fig. 1. *In situ* co-detection of diverse subtypes of aneuploid CTCs and CTECs expressing endogenous PD-L1 and Vimentin in NSCLC patients by SE-iFISH

(A) Heterogeneous localization of intracellular PD-L1 and Vimentin in different types of cultured cancer cells. **(A–a)** PD-L1 has a distinct distribution on the plasma membrane of a HCC HepG2 cell (IFI: medium). Vimentin is observed in the cytoplasm of HCC cells. **(A–b)** A majority of PD-L1 (green, IFI: high) localize on the nuclear envelope, and partly in the nucleus of a NSCLC A549 lung cancer cell. **(A–c)** Nuclear localization of PD-L1 is observed in an A549 cell (IFI: high). Vimentin shows a similar intracellular distribution in A-b/c. **(B)** *In situ* phenotypic and karyotypic characterization of aneuploid CTCs and CTECs enriched from NSCLC patients. **(B–a)** A large multiploid CTC (≥tetrasomy 8, $CD45^-/CD31^-/Vimentin^-$) has a positive staining for PD-L1 (IFI: high) in the patient P1 at PD. An attached WBC ($CD45^+$) is indicated by a red arrow. **(B–b)** A mesenchymal small $_S$CTC (≤WBC), with a phenotype of $CD31^-/PD\text{-}L1^-/Vimentin^+$, shows trisomy 8 in the cell of the patient P6 at baseline. **(B–c)** A CTM containing two aneuploid CTCs displays a scattered vesicle-like staining of PD-L1 in the nuclei and partially in the cytoplasm (IFI: low) in the patient P11 at baseline. **(B–d)** A multiploid CTEC ($CD45^-/CD31^+/Vimentin^-$) reveals positive expression of PD-L1 (green arrow, IFI: high) in the patient P1 at PD. Adjacent WBCs ($CD45^+$) are indicated by a red arrow. **(B–e)** A CTEC cluster consisting of several aneuploid CTECs is found to have PD-L1 expressed (IFI: high) in the patient P8 at PD. An attached mesenchymal WBC ($CD45^+/Vimentin^+$) is indicated by a red arrow. **(B–f)** A haploid mesenchymal CTEC ($CD31^+/PD\text{-}L1^-$) has Vimentin strongly expressed in the patient P11 at PD. **(B–g)** A mesenchymal CTEC cluster consisting of 5 diploid CTECs shows a phenotype of $CD31^+/PD\text{-}L1^-/Vimentin^+$ in the patient P5 at baseline. **(C)** CTC-CTEC fusion cluster (Epi-Endo fusion cluster): an aneuploid non-mesenchymal (Vim^-) cell cluster expressing both CD31 and EpCAM in a NSCLC patient is revealed. Bars: 5 μm.

2.3. Tri-marker-iFISH®

Six-channel tri-marker (PD-L1/Vimentin/CD31)-iFISH was performed according to the manufacture's updated protocol (Cytelligen) [16]. Briefly, dried monolayer cells on the coated slides were rinsed and incubated with PBS at room temperature for 3 min, followed by hybridization with Vysis chromosome 8 centromere probe (CEP8) SpectrumOrange (Abbott Laboratories, Chicago, IL, USA), approved by the USFDA to identify aneuploid solid tumor cells, for 4 h using a S500 StatSpin ThermoBrite Slide Hybridization/Denaturation System (Abbott Molecular, Abbott Park, IL, USA). Samples were subsequently incubated with the indicated post-fluorescence labeled monoclonal antibodies at 1: 200 dilution, including Alexa Fluor (AF)594-CD45 (ATCC, Manassas, VA, USA, Clone 9.4,), AF488-PD-L1 (Dana-Farber Cancer Institute, Harvard Medical School, Boston, MA, USA, Clone 29E.2A3), Cy5-CD31(Abcam, Burlingame, CA, USA, Clone EP3095), and Cy7-Vimentin (Abcam, Clone EPR3776) at room temperature for 20 min in dark [35]. After washing, samples were mounted with mounting media containing DAPI (blue) (Vector Laboratories, Burlingame, CA, USA), and subsequently subjected to automated 3D CTC image scanning and analyses. Direct conjugation of all different fluorescent dyes to the applied diverse antibodies was accomplished at Cytelligen.

2.4. Automated 3D scanning and image analysis of aneuploid CTCs and CTECs performed by Metafer-i•FISH®

Coated slides containing aneuploid CTCs and CTECs stained by iFISH were scanned by means of an automated Metafer-i•FISH® CTC 3D scanning and image analyzing system newly co-developed by Carl Zeiss (Oberkochen, Germany), MetaSystems (Altlussheim, Germany) and Cytelligen [16]. CTC slides were automatically loaded on a Zeiss fluorescence microscope (AXIO Imager Z2), and afterwards subjected to automated X–Y scanning with cross Z-sectioning of all cells performed at 1 μm steps of depth. X-Y-Z 3D scanning was performed in each of the 6 fluorescence color channels. Positive target cells are defined as $DAPI^+/CD45^-/PD\text{-}L1^{+\ or\ -}/Vim^{+\ or\ -}/CD31^{+\ or\ -}$ with diploid or aneuploid chromosome 8.

Following high through-put scanning, acquiring and processing cell images, subsequent comprehensive characterization and classification of $CD31^-$ CTCs and $CD31^+$ CTECs as well as statistical analyses were performed upon phenotypic, karyotypic and cell morphological characterization of the tri-element in the intracellular bio-chain [15], with particular focus on cell size, cell cluster, quantified immunostaining intensity of PD-L1 and Vimentin, as well as ploidy of chromosome 8, etc.

2.5. Statistical analyses

All statistical analyses were performed with IBM SPSS Statistics 25.0 (Armonk, NY, USA). Chi-squared tests and Fisher's exact tests were applied to compare categorical data. Positive correlation of CTCs and CTECs expressing PD-L1 with immunotherapy efficacy was analyzed using Fisher's exact test. Unpaired student's t-test and one-way analysis of variance (ANOVA) were applied to statistically analyze the difference between 2 groups, as well as the difference among 3 groups of separate data. Mann-Whitney *U* test was used to analyze proportion changes of morphology and karyotype in post-therapeutic CTCs and CTECs. Kaplan-Meier survival plots for PFS were generated upon the numbers of diverse subtypes of $PD\text{-}L1^{+/-}$ CTCs and CTECs. Survival curves were compared using log-rank tests. All *p* values were two-sided. $*p < 0.05$ and $**p < 0.01$ are statistically significant and very significant, respectively. PFS is defined as the duration from initial blood collection to the date disease progression was confirmed or censored at evaluation of immunotherapy efficacy. Sankey diagram was plotted utilizing the RStudio software v8.10 (Boston, MA, USA).

3. Results

3.1. In situ co-detection of aneuploid CTCs and CTECs expressing PD-L1 and Vimentin by SE-iFISH

Intracellular heterogeneous distribution of endogenous PD-L1 and Vimentin in different types of cancer cells, including the indicated hepatocellular carcinoma cells (HCC) HepG2 and non-small cell lung cancer cells A549, was co-examined by immunofluorescence (IF) staining. The amount of expressed PD-L1 is quantified by immunofluorescence intensity (IFI). Distribution of PD-L1 on the plasma membrane of a majority of HepG2 cells was revealed in Fig. 1A–a (IFI: medium). Shown in Fig. 1A and b, unlike HCC HepG2 cells, PD-L1 heterogeneously localized on the nuclear envelope or in the nuclei

Table 1
Clinical characteristics of the immunotherapeutic NSCLC patients.

Patient	Pathology	TNM Staging	Nivolumab		hPD-L1$^+$	Prior to immunotherapy		Completed immunotherapy
			1st	2nd		PD-L1$^+$ CTC	PD-L1$^+$ CTEC	
P1	ADC	IV		+	–	+	–	+
P2	ADC	IV		+	–	–	–	+
P3	SCC	IIIA		+	+	–	–	–
P4	ADC	IVB		+	+	–	–	–
P5	ADC	IIIB		+	–	–	–	+
P6	ADC	IVB		+	–	+	–	+
P7	NSCLC	IV		+	–	–	–	+
P8	ADC	IVB		+	–	–	–	+
P9	ADC	IVB		+	–	–	–	+
P10	SCC	IV		+	+	+	+	–
P11	SCC	IV		+	–	+	+	+
P12	SCC	IVB		+	+	+	–	+
P13	SCC	IVB		+	+	–	–	–
P14	ADC	IVA		+	n/a*	–	–	–
P15	SCC	IVB	+		n/a*	+	+	ongoing
P16	SCC	IV	+		–	+	–	ongoing
% of PD-L1$^+$ cells in hPD-L1$^+$ patients prior to nivolumab treatment (*excluded)						40.0%	20.0%	
% of PD-L1$^+$ cells in hPD-L1$^-$ patients prior to nivolumab treatment (*excluded)						44.4%	11.1%	
% of PD-L1$^+$ cells in overall patients prior to nivolumab treatment (*included)						43.8%	18.8%	

ADC, adenocarcinoma; SCC, squamous cell carcinoma; hPD-L1, histopathological PD-L1 expression.
1st, first-line nivolumab treatment; 2nd, second-line nivolumab treatment (failed first-line chemotherapy).
P7 NSCLC: pathology classification is not available due to histopathological complexity.

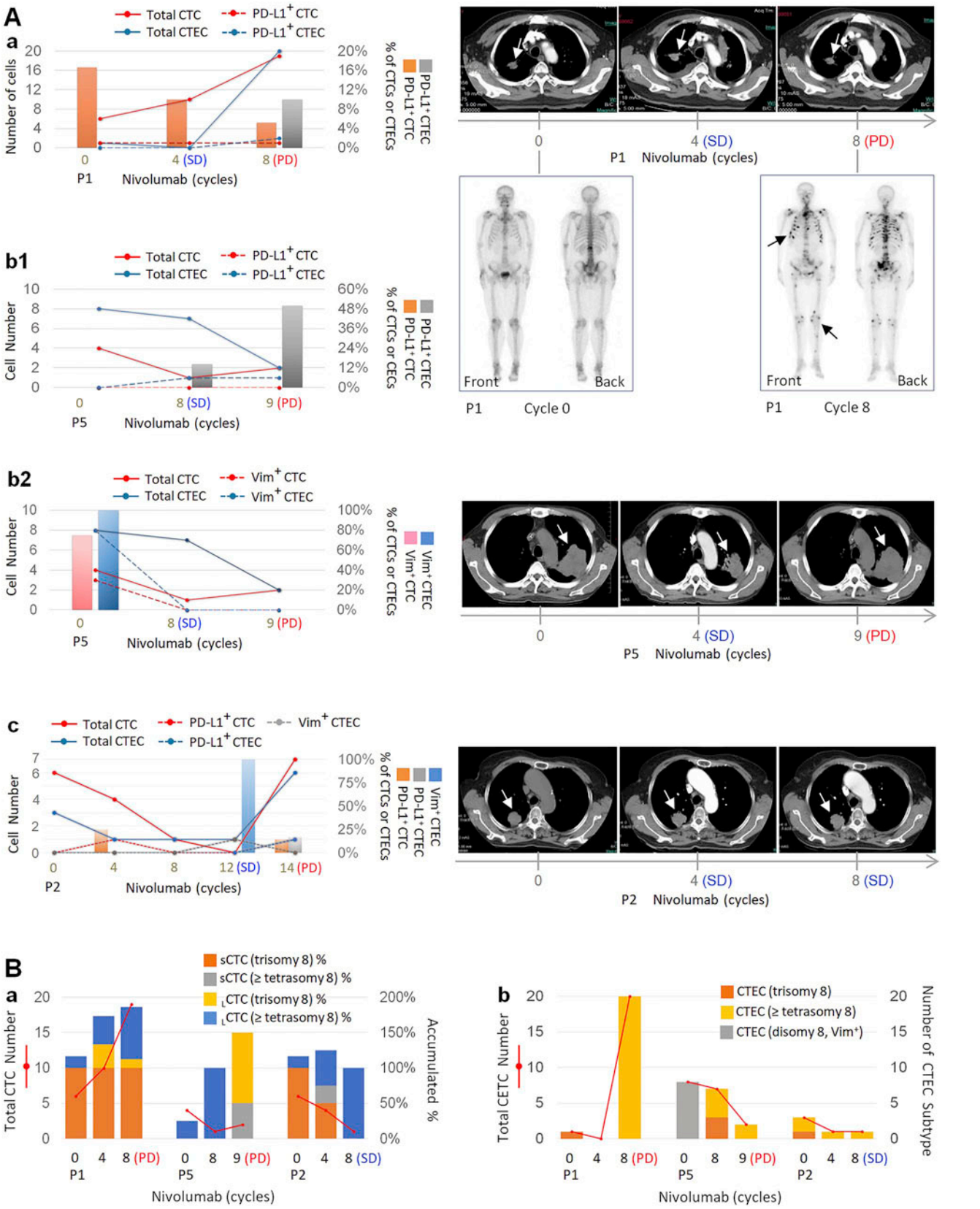

(caption on next page)

Fig. 2. Individual case analysis of PD-L1$^+$ or Vimentin$^+$ aneuploid CTCs and CTECs in NSCLC patients subjected to nivolumab treatment
(A-a) Patient P1 has PD at cycle-8 with newly developed cancer metastasis to bone (black arrows), but no enlargement of primary lesion is observed (white arrows). At cycle-8, the subject shows increased quantity of both overall aneuploid CTCs (from baseline 6 to 19 cells at PD, red line, left Y-axis) and CTECs (from 0 to 20 cells, blue line). Percentage of PD-L1$^+$ CTCs (PD-L1$^+$ CTCs *vs* overall CTCs, orange bar, right Y-axis) decreases following immunotherapy. Percentage of PD-L1$^+$ CTECs (PD -L1$^+$ CTECs *vs* overall CTECs, grey bar) enhances from 0 to 10% at PD. No Vim$^+$ CTC or CTEC is detected either before or during nivolumab therapy. **(A-b1)** Patient P5 (PD at cycle-9) shows an enlarged primary lesion without new distant metastasis. At cycle-9, reduced quantity for both aneuploid overall CTCs (from baseline 4 cells to 2 cells, red line) and CTECs (from 8 to 2 cells, blue line) is revealed, whereas percentage of PD-L1$^+$ CTECs increases from 14 at cycle-8 to 50% at cycle-9 (grey bar). **(A-b2)** All baseline Vimentin$^+$ aneuploid CTCs (3 cells, red dot line; 75%, pink bar), and Vim$^+$ CTECs (8 cells, blue dot line; 100%, blue bar) are eliminated at PD. **(A–c)** Patient P2 has maintained stable disease (SD) status throughout first 12 therapy cycles, and quantity of all the CTCs (baseline 6 cells, red line) and CTECs (baseline 3 cells, blue line) decreases during 12 cycles treatment (SD). The patient has 1 aneuploid CTEC detected at cycle-12 (grey dash line), which is Vimentin$^+$ (1/1 = 100%, blue bar). At cycle-14 (PD), the number of both CTCs and CTECs respectively increases to 7 (red line) and 6 cells (blue line), containing 1 PD-L1$^+$ CTC (red dash line, 1/7 = 14.3%, orange bar) and 1 PD-L1$^+$ CTEC (blue dash line, 1/6 = 16.7%, grey bar). **(B)** Karyotypic and morphological analyses of aneuploid CTCs and CTECs. Patient P1 shows that most of increased CTCs (B-a, P1, blue) and CTECs (B-b, P1, yellow) at PD are multiploid (≥tetrasomy 8). With respect to patient P5 at the time of PD, a majority of CTCs are triploid $_L$CTCs (B-a, P5, yellow), and most of CTECs are multiploid (B-b, P5, yellow). Regarding patient P2 at SD (8 cycles), karyotype and morphology shifting from baseline triploid $_S$CTCs to multiploid $_L$CTCs following nivolumab treatment is observed (B-a, P2). Quantity of CTECs is minimized during the therapy (B-b, P5, 1 multiploid cell).

(Fig. 1A–c) of the most NSCLC A549 cells (IFI: high). Vimentin showed an intracellular distribution in HepG2 and A549 cells (Fig. 1A, a-c). Both nuclear localization of PD-L1 and positive expression of Vimentin in A549 cells revealed in this study keeps in accordance with the report published by others, showing that nuclear PD-L1 (nPD-L1) was expressed in Vimentin$^+$ mesenchymal CTCs in colorectal and prostate cancer patients undergoing therapy [31].

Six-channel tri-marker-iFISH was applied to perform *in situ* phenotypic and karyotypic characterization of aneuploid CTCs (CD31$^-$/CD45$^-$) and CTECs (CD31$^+$/CD45$^-$) enriched by SE from immunotherapeutic NSCLC patients.

Shown in Fig. 1B–a, a large multiploid CTC (≥tetrasomy 8) displayed a CD31$^-$/PD-L1$^+$/Vim$^-$ phenotype (PD-L1 IFI: high). Displayed in Fig. 1B–b, a small (≤5 μm WBC) mesenchymal triploid CTC was CD31$^-$/PD-L1$^-$/Vim$^+$. A circulating tumor microemboli (CTM) revealed in Fig. 1B–c had 2 multiploid CD31$^-$ CTCs. Scattered, vesicle-like staining of PD-L1 (IFI: low) was observed in nuclei and partially in cytoplasm of CTM. This suggests that besides possible on-going trafficking of nuclear translocation, some intracellular PD-L1 might also be in the cytoplasmic secretary vesicles and secreted along either a constitute or a regulatory pathway [36], turning into functional soluble PD-L1 in sera [37].

A CD31$^+$ aneuploid CTEC and a CD31$^+$ CTEC cluster were illustrated in Fig. 1B–d and e, respectively, both were multiploid and positive for PD-L1 staining (IFI: high). Shown in Fig. 1B–f, a mesenchymal CTEC (CD31$^+$/Vim$^+$/PD-L1$^-$) displayed a haploid Chr 8. In Fig. 1B–g, a mesenchymal circulating endothelial cell cluster consisted of 5 diploid Vim$^+$/PD-L1$^-$ endothelial cells.

Extending our previous study, which showed aneuploid Vim$^+$ mesenchymal CTC-CTEC fusion clusters in diverse types of cancer patients [16], an aneuploid, non-mesenchymal (Vim$^-$) CTC-CTEC fusion cluster (Epi-Endo fusion cluster) expressing both the epithelial marker EpCAM and the endothelial marker CD31 in a lung cancer patient was displayed in Fig. 1C. Given the vital significance of EpCAM on CTCs [13,33,38], it would be significant to further probe both mesenchymal and non-mesenchymal fusion clusters, which will help further understand how tumor cells (TCs) interact with TECs during the process of EMT/MET (intravasation/extravasation) [14] or implantation of cancer cells, how CTCs interplay with CTECs in peripheral circulation, and what the potential clinical utilities of CTC-CTEC fusion clusters have.

3.2. Individual case analysis of aneuploid CTCs and CTECs detected in patients

Optimized SE-iFISH, along with nivolumab therapy, was performed to periodically detect PD-L1$^+$/Vimentin$^+$ aneuploid CTCs and CTECs in NSCLC patients. Information of the enrolled patients, including histopathological needle biopsy examination of PD-L1 expression (hPD-L1), was summarized in Table 1. All the patients who were subjected to second-line nivolumab treatment failed first-line chemotherapy.

Patient P1: Depicted in Fig. 2A–a, the patient had PD at nivolumab therapy cycle-8, showing post-immunotherapeutic cancer distant metastasis to bone throughout the whole body (black arrows). No obvious enlargement of the primary lesion was observed (white arrows). Following development of PD at cycle-8, the patient showed an increase in the number of total aneuploid CTCs (red line) and CTECs (blue line). Moreover, in contrast to the percentage of PD-L1$^+$ CTCs (PD-L1$^+$ CTCs *vs* total CTCs, orange bar), the percentage of PD-L1$^+$ CTECs (PD-L1$^+$ CTECs *vs* overall CTECs, grey bar) increased at PD. Further analysis demonstrated that, most of the increased CTCs (Fig. 2B–a, P1, blue) and CTECs (Fig. 2B–b, P1, yellow) in patient P1 were multiploid (≥tetrasomy 8). No Vim$^+$ CTC or CTEC was detected either prior to or during nivolumab therapy.

Patient P5: Revealed in Fig. 2A-b1, the quantity of total aneuploid CTCs (baseline 4 cells, red line), and total CTECs (baseline 8 cells, blue line) reduced to 2 cells at PD (treatment cycle-9). Similarly, shown in Fig. 2A-b2, Vim$^+$ aneuploid CTCs (baseline 3 cells, red dot line), and Vim$^+$ CTECs (baseline 8 cells, blue dot line) were eliminated following nivolumab therapy. The patient showed an increased size of the primary lesion (white arrows) without distant metastasis at PD (cycle-9). Increased percentage of PD-L1$^+$ CTECs (PD-L1$^+$ CTECs *vs* total CTECs) was found at PD. Karyotype analysis indicated that at PD, a majority of remaining CTCs were triploid large $_L$CTCs (> 5 μm WBC) (Fig. 2B–a, P5, yellow), and CTECs were multiploid (Fig. 2B–b, P5, yellow).

Patient P2: Illustrated in Fig. 2A–c, the patient maintained a stable disease (SD) status throughout first 12 therapy cycles, and had PD at cycle-14. The number of CTCs (baseline 6 cells, red line) and CTECs (baseline 3 cells, blue line) decreased until cycle-12. At cycle-14 (PD), both total CTCs and CTECs increased to 7 and 6 cells, respectively. One of the seven CTCs at cycle-14 was PD-L1$^+$ (1/7 = 14.3%), and 1 of the 6 CTECs showed PD-L1$^+$ (1/6 = 16.7%). Only 1 CTEC was detected at cycle-12, which was Vim$^+$ mesenchymal CTEC (1/1 = 100%). To demonstrate post-immunotherapeutic karyotype and morphology shifting of CTCs and CTECs in different PD as well as SD patients, analyses were performed on above 3 patients normalized to the similar 8~9 treatment cycles, including P1 with new metastasis, P5 with enlarged primary lesion, and P2 at SD stage (cycle-8). Depicted in Fig. 2B–a, patient P2 at cycle-8 (SD) showed a majority of baseline triploid small $_S$CTCs shifting to multiploid $_L$CTCs following nivolumab treatment. Further analyses of all CTCs and CTECs in patients receiving complete courses of immunotherapy are described below.

3.3. Comprehensive analysis of all the aneuploid CTCs and CTECs detected in NSCLC patients subjected to second-line nivolumab therapy

Non-hematologic aneuploid circulating rare cells (CRCs) are mainly composed of aneuploid CTCs (CD31$^-$/CD45$^-$) and CTECs (CD31$^+$/CD45$^-$) [15]. Compositional analysis illustrated in Fig. 3A demonstrated that,

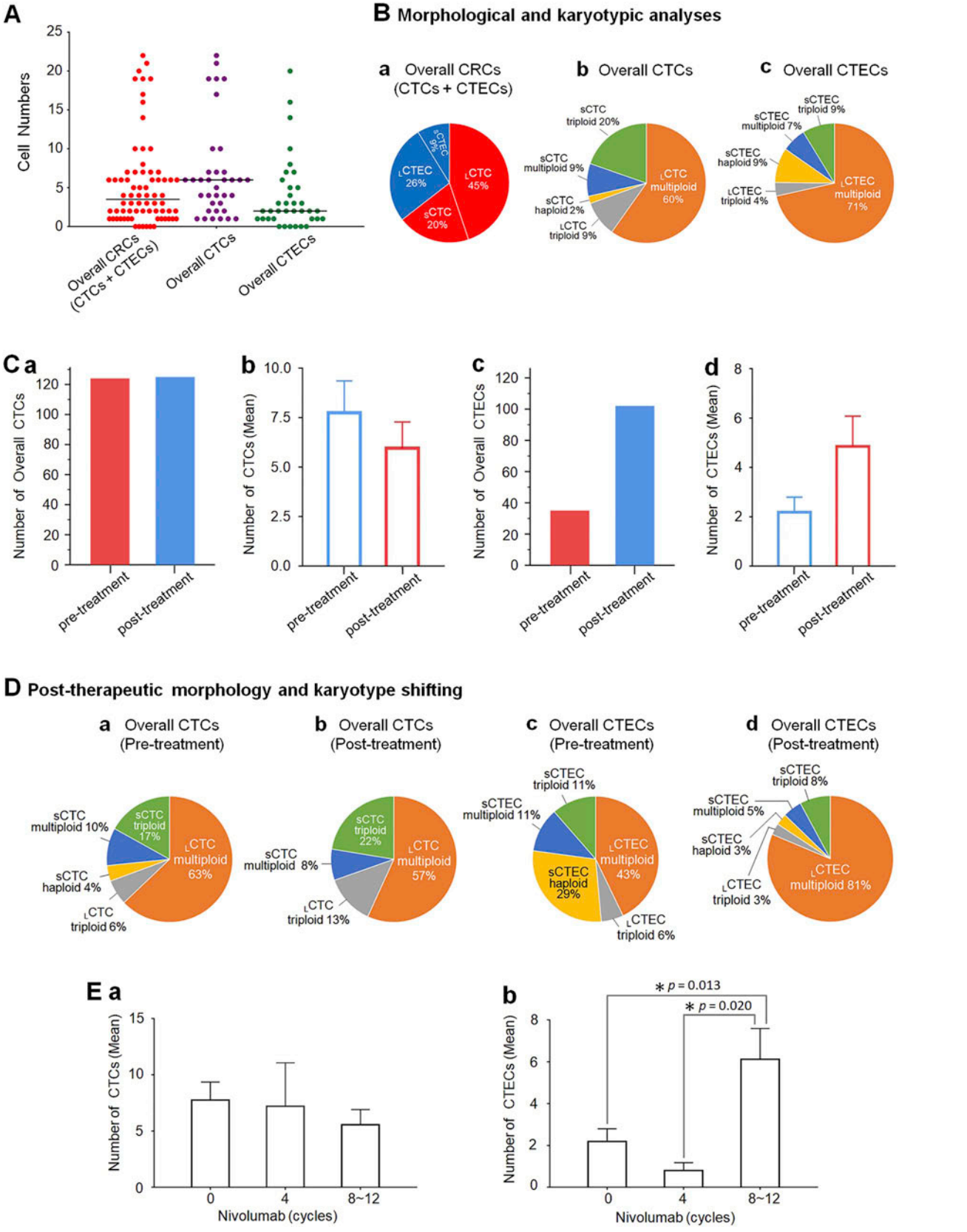

(caption on next page)

Fig. 3. Comprehensive analysis of aneuploid CTCs and CTECs detected in overall pre- and post-immunotherapeutic NSCLC patients
(A) Compositional analysis: Out of a total of 386 pre- and post-treatment aneuploid CRCs (CTCs + CTECs), there are 249 CTCs with a median of 6 cells (black line) (Min 1/Max 22), and 137 CTECs with a median of 2 cells (Min 0/Max 20). **(B–a)** Morphological analysis of overall CRCs: among all the detected aneuploid CRCs, 65% are CTCs, broken down into 45% large $_L$CTCs (> 5 μm WBC) and 20% small $_S$CTCs (≤ 5 μm WBC); remaining 35% of overall CRCs are aneuploid CTECs, consisting of 26% $_L$CTECs and 9% $_S$CTECs. (**B-b/c**) Karyotype analysis of overall CTCs and CTECs: multiploid (≥ tetrasomy 8) large cells constitute the majority of the population for both CTCs (60%) and CTECs (71%). **(C)** Quantification analysis (Mean ± SEM). (C-a/b, CTCs): a total of 16 patients have 124 pre-treatment baseline CTCs (red, mean = 7.75 ± 1.61) and 125 post-therapeutic CTCs (blue, mean = 5.95 ± 1.33) detected (p = 0.392, T-test). (C-c/d, CTECs): a total of 35 pre-treatment CTECs (red, mean = 2.19 ± 0.61), and 102 overall post-therapeutic CTECs (blue, mean = 4.86 ± 1.23) are identified in the same cohort of patients (p = 0.061, T-test). **(D)** Post-therapeutic morphology and karyotype shifting in overall pre- and post-immunotherapeutic patients. (D-a/b, CTCs): Following anti-PD-1 treatment, depletion of haploid $_S$CTCs (yellow) and increased proportions of triploid $_L$CTCs (from 6% to 13%, grey) and $_S$CTCs (17% to 22%, green) are observed. (D-c/d, CTECs): Compared to the amount of pre-treatment CTECs, a decreased percentage of haploid $_S$CTECs from 29% to 3% (p = 0.498, Mann-Whitney U test), and a dramatically increased percentage of multiploid $_L$CTECs (from 43% to 81%, orange) are revealed. Increase of multiploid $_L$CTECs following immunotherapy is statistically very significant (**p = 0.004 < 0.01, Mann-Whitney U test). **(E)** Statistical analysis of CTCs and CTECs quantified at the indicated treatment intervals (Mean ± SEM). (E-a, CTCs): Quantified overall CTCs have the means of 7.8 ± 1.61, 7.2 ± 3.87 and 5.6 ± 1.35 CTCs detected at 0, 4, and 8~12 treatment cycles, respectively. No significant difference is revealed (p = 0.614, F = 0.495, ANOVA test). (E-b, CTECs): Quantification of CTECs performed at the same intervals along the nivolumab treatment cycles shows the means of 2.2 ± 0.61, 0.8 ± 0.37 and 6.1 ± 1.45 CTECs. Differences of CTEC mean numbers between cycle 0 and cycles 8~12 (*p = 0.013 < 0.05, ANOVA test), cycle 4 and cycles 8~12 (*p = 0.020 < 0.05, ANOVA test) are statistically significant.

a total of 386 overall aneuploid CRCs (CTCs + CTECs) were detected in 37 blood samples from 16 enrolled NSCLC patients. Out of 386 cells, 249 were CTCs, with a minimum detection number of 1, and a maximum detection number of 22 cells. The median of the detected CTC number was 6. The remaining 137 CRCs were CTECs with a median of 2 cells (Minimum 0/Maximum 20).

Depicted in Fig. 3B–a, morphological analysis indicated that 65% of overall aneuploid CRCs were CTCs, comprising of 45% large $_L$CTCs (> 5 μm) and 20% small $_S$CTCs (≤ 5 μm WBC). The remaining 35% of CRCs were aneuploid CTECs, containing 26% large $_L$CTECs and 9% small $_S$CTECs. Further karyotype analysis (Fig. 3B-b/c) revealed that multiploid (≥ tetrasomy 8) large cells constitute the main population for both aneuploid CTCs ($_L$CTC, 60%) and aneuploid CTECs ($_L$CTEC, 71%).

Quantitative, morphological and karyotypic analyses were performed to comprehensively investigate CTCs and CTECs detected in 16 patients. Illustrated in Fig. 3C–a, total of 124 baseline CTCs in all the 16 pre-treatment patients and 125 CTCs in 21 post-therapy specimens were respectively detected in the subjects. Fig. 3C–b showed a mean of 7.75 ± 1.61 CTCs (Mean ± SEM) for pre-treatment patients, and a mean of 5.95 ± 1.33 CTCs for post-therapeutic subjects. The difference between the mean values of pre- and post-treatment was not statistically significant (p = 0.392, T-test). Revealed in Fig. 3C-c/d, 35 of pre- and 102 of post-therapy CTECs were detected in the same cohort of patients, with a mean of 2.19 ± 0.61 (pre-treatment) and 4.86 ± 1.23 CTECs (post-treatment), respectively. Though quantity of post-therapeutic CTECs increased 3 times compared to that of pre-treatment, the difference between the mean values did not reach statistical significance in this study (p = 0.061, T-test).

Morphology and karyotype shifting in both CTCs and CTECs was observed in patients following immunotherapy. Demonstrated in Fig. 3D-a/b, compared to the overall pre-treatment CTCs, all the haploid $_S$CTCs were eliminated in post-treatment patients. Also noted was an increased percentage in triploid CTCs, including both small (from 17% to 22%, green) and large cells (from 6% to 13%, grey). Depicted in Fig. 3D-c/d, the percentage of haploid $_S$CTECs decreased from 29% to 3% following immunotherapy (p = 0.498, Mann-Whitney U test), and a decreased percentage was also observed in most of other post-therapeutic CTEC subtypes, but none of them was statistically significant. Only multiploid $_L$CTECs, however, increased from 43% (pre-treatment) to 81% (post-treatment), proving to be very statistically significant (**p = 0.004 < 0.01, Mann-Whitney U test). Proportional correlation of aneuploid chromosome copy numbers with malignancy degree of breast carcinoma cells was published by others [39].

Despite the limited specimen quantity, obtained results suggested that anti-PD-1 treatment could facilitate the elimination of small haploid CTCs and reduction in the percentage of small haploid CTECs, whereas multiploid $_L$CTECs seemed to have a resistance to nivolumab, as shown in the significantly increased percentage in NSCLC patients following therapy. Interestingly, intrinsic resistance of triploid CTCs to the chemotherapeutic agent cisplatin in gastric cancer patients was previously reported [40].

To verify the unique characteristics of CTECs with respect to resistance to anti-PD-1 therapy, statistical analysis was performed on the target cells detected at the indicated treatment intervals. Shown in Fig. 3E–a, an analysis of overall CTCs detected at the indicated time

Table 2
Analysis of post-therapeutic aneuploid CTCs and CTECs in advanced NSCLC patients subjected to second-line immunotherapy.

Patients hPD-L1$^+$		apCTCs			apCTECs			Progressive Disease		
		Overall	PD-L1$^+$	Vim$^+$	Overall	PD-L1$^+$	Vim$^+$	Treat. cycles prior to PD	Enlarg. Prim. tumor	New metastases
P1	–	↑	+	–	↑	+	–	8	–	+
P2	–	↑	+	–	↑	+	+	14	+	–
P5	–	↑	–	+*	↑	+	–	9	+	–
P6	–	no change	+*	+*	no change	–	+*	8	–	+
P7	–	↑	–	–	↑	+	–	12	+	–
P8	–	↓	–	–	↑	+	–	8	–	+
P9	–	↑	–	–	↓	+	–	12	+	+
P11	–	no change	+*	–	↑	+	+	12	–	+
P12	+	↓	+*	–	↑	–	–	12	–	+
SUM	Post-therapy (PD-L1$^+$)		2			7				
	Prior to therapy (PD-L1$^+$)		4 (Table 1, excluding P10, 15, 16)			1 (Table 1, excluding P10, 15)				
p value (X^2)			p = 0.617 (X^2 = 0.250, PD-L1$^+$ CTCs)			*p = 0.018 (X^2 = 5.625, PD-L1$^+$ CTECs)				

↑ number of cells increases; ↓ number of cells decreases; + positive detection; - negative detection.
+* positive detection prior to nivolumab treatment (baseline, cycle 0), but negative following therapy.

point showed the means of 7.8 ± 1.61, 7.2 ± 3.87 and 5.6 ± 1.35 (Mean ± SEM) CTCs at 0, 4, and 8~12 therapy cycles, respectively. Differences in means of CTC quantities were not statistically significant ($p = 0.614$, F = 0.495, ANOVA test). Depicted in Fig. 3E–b, quantification of CTECs detected at the same nivolumab therapy intervals revealed the means of 2.2 ± 0.61, 0.8 ± 0.37 and 6.1 ± 1.45 CTECs, respectively. ANOVA test showed statistically significant differences of the CTEC mean values between cycle 0 and cycles 8~12 ($*p = 0.013 < 0.05$), cycle 4 and cycles 8~12 ($*p = 0.020 < 0.05$), respectively. Obtained results indicated that a statistically significant increase of CTECs in PD patients was relevant to anti-PD-1 resistance.

3.4. Categorical analysis of PD-L1$^+$ CTCs and CTECs in immunotherapeutic patients

Revealed in Table 1, among 5 of pre-treatment histopathological hPD-L1$^+$ patients, 2 had PD-L1$^+$ CTCs (2 out of 5, 40%). Out of 9 hPD-L1$^-$ subjects, 4 showed PD-L1$^+$ CTCs (4 out of 9, 44.4%). Positive detection rate for PD-L1$^+$ CTECs in those patients was 20% (1 out of 5 hPD-L1$^+$) and 11.1% (1 out of 9 hPD-L1$^-$), respectively. Among a total of 16 enrolled patients, 43.8% (7 out of 16) had PD-L1$^+$ CTCs and 18.8% (3 out of 16) had PD-L1$^+$ CTECs. Obtained results indicated that PD-L1$^+$ CTCs and CTECs could be effectively detected in both hPD-L1$^+$ and hPD-L1$^-$ subjects. This keeps in accordance with the published results of our previous study, demonstrating that a significant amount of HER2$^+$ CTCs were detected in hHER2$^-$ gastric cancer patients [11].

Out of the 16 enrolled patients in Table 1, 5 subjects were unable to receive complete nivolumab treatment due to patients' death or severe sickness, 2 on-going patients underwent immunotherapy, and the remaining 9 subjects, who received entire courses of second-line anti-PD-1 therapy, eventually had PD following different cycles of nivolumab treatment (Table 2).

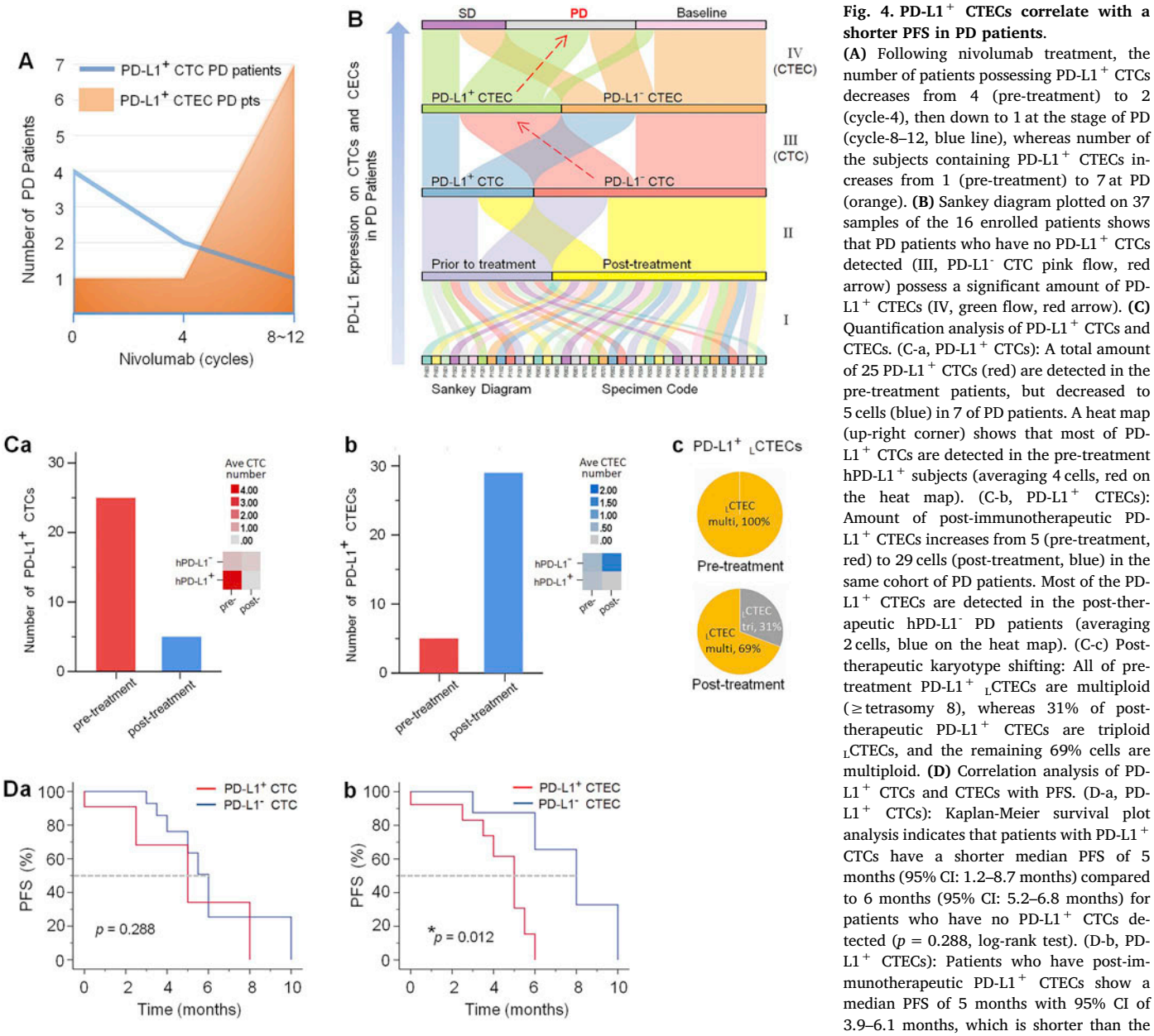

Fig. 4. PD-L1$^+$ CTECs correlate with a shorter PFS in PD patients.
(A) Following nivolumab treatment, the number of patients possessing PD-L1$^+$ CTCs decreases from 4 (pre-treatment) to 2 (cycle-4), then down to 1 at the stage of PD (cycle-8–12, blue line), whereas number of the subjects containing PD-L1$^+$ CTECs increases from 1 (pre-treatment) to 7 at PD (orange). **(B)** Sankey diagram plotted on 37 samples of the 16 enrolled patients shows that PD patients who have no PD-L1$^+$ CTCs detected (III, PD-L1$^-$ CTC pink flow, red arrow) possess a significant amount of PD-L1$^+$ CTECs (IV, green flow, red arrow). **(C)** Quantification analysis of PD-L1$^+$ CTCs and CTECs. (C-a, PD-L1$^+$ CTCs): A total amount of 25 PD-L1$^+$ CTCs (red) are detected in the pre-treatment patients, but decreased to 5 cells (blue) in 7 of PD patients. A heat map (up-right corner) shows that most of PD-L1$^+$ CTCs are detected in the pre-treatment hPD-L1$^+$ subjects (averaging 4 cells, red on the heat map). (C-b, PD-L1$^+$ CTECs): Amount of post-immunotherapeutic PD-L1$^+$ CTECs increases from 5 (pre-treatment, red) to 29 cells (post-treatment, blue) in the same cohort of PD patients. Most of the PD-L1$^+$ CTECs are detected in the post-therapeutic hPD-L1$^-$ PD patients (averaging 2 cells, blue on the heat map). (C-c) Post-therapeutic karyotype shifting: All of pre-treatment PD-L1$^+$ $_L$CTECs are multiploid (≥ tetrasomy 8), whereas 31% of post-therapeutic PD-L1$^+$ CTECs are triploid $_L$CTECs, and the remaining 69% cells are multiploid. **(D)** Correlation analysis of PD-L1$^+$ CTCs and CTECs with PFS. (D-a, PD-L1$^+$ CTCs): Kaplan-Meier survival plot analysis indicates that patients with PD-L1$^+$ CTCs have a shorter median PFS of 5 months (95% CI: 1.2–8.7 months) compared to 6 months (95% CI: 5.2–6.8 months) for patients who have no PD-L1$^+$ CTCs detected ($p = 0.288$, log-rank test). (D-b, PD-L1$^+$ CTECs): Patients who have post-immunotherapeutic PD-L1$^+$ CTECs show a median PFS of 5 months with 95% CI of 3.9–6.1 months, which is shorter than the median PFS of 8 months (95% CI: 4.9–11 months) for patients who have no PD-L1$^+$ CTECs detected. The difference between the median PFS is statistically significant ($*p = 0.012 < 0.05$, log-rank test).

3.5. Positive detection of PD-L1$^+$ CTECs correlates with a shorter PFS in PD patients

Described in Table 2, 9 patients who underwent 8~14 nivolumab treatment cycles had PD, showing either enlarged primary tumor size or development of new metastatic lesions. Among those 9 PD patients, 5 out of 9 subjects (55.6%) had an increased quantity of overall aneuploid CTCs. None of PD patients had detectable post-therapeutic Vim$^+$ CTCs. With respect to aneuploid CTECs, an enhanced amount of overall CTECs was found in 7 out of 9 PD subjects (77.8%), and 2 of PD patients had Vim$^+$ CTECs detected. Obtained results suggested that increased CTCs and CTECs might be relevant to nivolumab resistance and progression of disease in post-immunotherapeutic patients.

Further analysis was performed to examine whether the specific subtype of CTC or CTEC expressing PD-L1 had a significant impact on immunotherapy resistance. Revealed in Table 2 and Fig. 4A, 2 patients had PD-L1$^+$ CTCs detected at the treatment cycle-4, compared to 4 pre-treatment patients who showed PD-L1$^+$ CTCs ($p = 0.617$, Chi-squared test). At the stage of PD (cycles 8~12), compared to 1 subject who had baseline PD-L1$^+$ CTEC detected prior to therapy, 7 out of 9 post-therapeutic PD patients showed a positive detection of PD-L1$^+$ CTECs. The difference between the number of pre- and PD patients (1 *vs* 7) was statistically significant (*$p = 0.018 < 0.05$, Chi-squared test). Only 1 PD subject had PD-L1$^+$ CTC detected at cycles 8~12 (Fig. 4A). Obtained results suggested that positive detection of post-therapeutic PD-L1$^+$ CTEC is relevant to anti-PD-1 resistance and development of PD in cancer patients, which was supported by a Sankey diagram analysis plotted on 37 samples of the 16 enrolled patients (Fig. 4B), showing that a significant amount of PD-L1$^+$ CTECs (IV, green flow, red arrow) were identified in those PD patients who had no PD-L1$^+$ CTCs detected (III, PD-L1$^-$ CTC pink flow, red arrow).

Quantification analysis depicted in Fig. 4C–a indicated that a total amount of 25 PD-L1$^+$ CTCs were detected in pre-treatment patients, but decreased to 5 cells in post-therapeutic PD patients. A heat map revealed that pre-treatment hPD-L1$^+$ subjects had most of the PD-L1$^+$ CTCs detected (averaging 4 cells). Demonstrated in Fig. 4C–b, the quantity of total post-immunotherapeutic PD-L1$^+$ CTECs increased from 5 (pre-treatment) to 29 cells (post-treatment) in the same cohort of PD patients. Most of the PD-L1$^+$ CTECs, averaging 2 cells, were detected in the post-therapeutic hPD-L1$^-$ PD patients as depicted in the heat map. Depicted in Fig. 4C–c, morphological and karyotypic analyses revealed that the entire population of pre-treatment PD-L1$^+$ CTECs were multiploid (≥tetrasomy 8) large cells ($_L$CTECs), and karyotype shifting was observed in post-therapeutic PD-L1$^+$ CTECs, showing 69% of multiploid $_L$CTECs and 31% of triploid $_L$CTECs in PD patients following immunotherapy.

Correlation of PD-L1$^+$ CTCs or CTECs with patients' progression-free survival (PFS) was analyzed utilizing Kaplan-Meier survival plots on 37 samples of 16 patients, including 9 PD subjects. Depicted in Fig. 4D–a, patients harboring PD-L1$^+$ CTCs (specimen quantity: 11) showed a shorter median PFS of 5 months (95% confidence interval CI: 1.2–8.7 months) compared to 6 months (95% CI: 5.2–6.8 months) for patients without PD-L1$^+$ CTCs (specimen quantity of 26). The difference in PFS was not statistically significant ($p = 0.288$, log-rank test). On the contrary, as shown in Fig. 4D–b, patients possessing PD-L1$^+$ CTECs (specimen quantity of 13) had a median PFS of 5 months (95% CI: 3.9–6.1 months), which was shorter than 8 months (95% CI: 4.9–11 months) for patients who had no PD-L1$^+$ CTECs detected (specimen quantity of 24). The difference between the values of median PFS was statistically significant (*$p = 0.012$, log-rank test), indicating that PD-L1$^+$ CTECs had a relevance to tumor progression and patients' shorter PFS.

4. Discussion

To investigate whether PD-L1 is expressed on aneuploid CTECs and its potential relative clinical impact, a novel integrated SE-iFISH strategy was established and optimized in the present study, to co-detect and comprehensively characterize CTCs and CTECs in advanced NSCLC patients subjected to second-line anti-PD-1 immunotherapy.

Aneuploidy (ap), the aberrant alternation (either gain or loss) of chromosomes in a cell, is an acceptable hallmark of malignant neoplastic cells [41,42]. Abnormal ploidy of chromosome(s) is proportional to malignancy status, illustrating that the higher copy number of chromosome, the higher malignancy degree [39]. It has been reported that chromosome aneuploidy in neoplastic cells impacts on transcription of multiple genes [43], resulting in a profound variety of phenotypes that subsequently contribute to tumor heterogeneity, therapy failure [44], cancer relapse [33], and therapeutic drug resistance in either patients [11,40], or metastatic PDX (mPDX) tumor animal models [45]. In the current study, centromere probe 8 (Vysis), the sole FISH probe approved by the USFDA to identify aneuploid solid tumor cells, was applied to detect non-hematologic CTCs and CTECs possessing aneuploid chromosome 8.

Similar to the conventional shedding process of the ordinary diploid circulating endothelial cells (CECs), some abnormal aneuploid tumor endothelial cells (TECs) [17,18], shed from tumor blood vessels into circulation, turning into CD31$^+$ aneuploid circulating tumor endothelial cells (CTECs) [15,16]. Alike the epithelial-to-mesenchymal transition (EMT) for CTCs, the inducible endothelial-to-mesenchymal transition (EndoMT) participates the process from TECs to CTECs [46], during which an acquired mesenchymal marker (such as Vimentin) is expressed in TECs or CTECs as displayed in Fig. 1B–f. It has been recognized that Vim$^+$ mesenchymal CTCs are associated with cancer progression, invasion and metastasis in a variety of cancer patients [47,48]. Clinical utilities of Vim$^+$ CTECs, and those CTECs that express a series of tumor biomarkers (HER2, EpCAM, PD-L1, etc.) as well as the stemness marker CD44v6 in carcinoma patients, remain to be investigated [23].

A positive association of increased PD-L1 expression with EMT in epithelial cancer cells was highlighted by others [49,50]. Previous studies demonstrated that down-regulation of plasma membrane associated PD-L1 and up-regulation of nuclear nPD-L1 involving PI3K/AKT pathway in neoplastic cells could be induced by chemotherapy in breast cancer (BCA) patients [51]. Additional studies indicated that nPD-L1 detected in Vim$^+$ mesenchymal CTCs in colorectal and prostate cancer patients undergoing first-line chemotherapy significantly associated with a shorter PFS or OS in patients, suggesting that nuclear translocated nPD-L1 had a great prognostic value for carcinoma patients [31]. The present study showed that regardless of negative expression of Vimentin, most of the aneuploid CTECs or CTCs detected in either pre- or post-immunotherapeutic NSCLC patients who were previously subjected to first-line chemotherapy, had a nuclear or perinuclear localization of PD-L1 as revealed in Fig. 1B, which is in accordance with that observed in chemotherapeutic BCA patients [51]. Several intriguing questions rise, including whether nuclear localization of nPD-L1 in tumor cells is cancer type-dependent as depicted in Fig. 1A (lung cancer *vs* HCC), whether and how Vimentin expression may interplay with chemotherapy to impact on nuclear translocation of nPD-L1 in lung cancer CTECs/CTCs, and the relevant clinical significance need to be further explored.

Differentially regulated PD-L1 expression on cancer cells, immune cells and angiogenesis related TECs attenuates anti-cancer immunity [27]. IFNγ activates TECs by inducing expression of PD-L1/PD-L2 on those cells, which subsequently down-regulates CD8$^+$ T cell cytolysis activity in a tumor microenvironment [6]. Despite a limited number of the enrolled patients, the current preliminary study demonstrated that, although nivolumab treatment could effectively deplete small cell size haploid CTCs and CTECs, a majority of multiploid PD-L1$^+$ CTECs showed resistance to second-line nivolumab therapy. Compared to the reduced number of PD patients who had post-therapeutic PD-L1$^+$ CTCs detected (Table 2), increased number of PD patients who had an augmented quantity of both overall CTECs and the particular subtype of

PD-L1$^+$ CTECs was observed (Table 2 and Fig. 4), indicating on-going angiogenesis and increased TECs in tumor lesions. Given that TECs are among the first contacts of infiltrating immune players in the tumor bed, an enhanced tumor vasculature barrier contributed by an increase in the quantity of TECs, may block transendothelial extravasation as well as infiltration of T-lymphocytes into the tumor microenvironment [52]. Moreover, PD-L1 on CTECs may bind to PD-1 on T cells and subsequently exert inhibitory impact on CD8$^+$ T cell cytolytic functions, resulting in reduced immunotherapy efficacy and a shorter PFS for carcinoma patients.

Besides post-therapeutic PD-L1 phenotype shifting, both CTCs and CTECs also underwent morphology and karyotype shifting following nivolumab treatment as revealed in Fig. 3D. In particular, a significant decrease in haploid $_S$CTECs and a dramatic increase in multiploid $_L$CTECs were observed in post-immunotherapeutic patients at the time of PD. Further analysis identified that the specific subtype of multiploid PD-L1$^+$ $_L$CTECs constituted the main population of the significantly increased CTECs following nivolumab therapy (Fig. 3D-c/d). Patients possessing multiploid PD-L1$^+$ CTECs were found to have a statistically significant shorter PFS compared to the subjects with no PD-L1$^+$ CTECs detected. In view of the fact that an increased abnormal copy number of aneuploid chromosome(s) in cancer cells is proportional to the malignancy degree [39], those elevated post-therapeutic multiploid PD-L1$^+$ CTECs may have higher degree of malignancy and associate with PD patients' shorter PFS. Obtained results suggest that PD-L1$^+$ multiploid ($\geq$tetrasomy 8) $_L$CTECs in post-immunotherapeutic PD patients may have "intrinsic resistance" to anti-PD-1 therapy, whereas PD-L1$^+$ triploid $_L$CTECs detected only in the post-therapy patients might be relevant to "induced resistance" (Fig. 4C–c). This is in line with our previous studies performed on either metastatic PDX tumor mouse models [45] or gastric cancer patients [11,40], showing that the specific subtype of CTCs were resistant to the chemotherapeutic agent cisplatin.

PD-L1$^+$ CTCs and PD-L1$^+$ CTECs may have different response mechanisms to anti-PD-1 therapy. Second-line immune checkpoint inhibitor (nivolumab) alone might not be sufficient to interfere or block PD-1 on T cells from binding to PD-L1 on CTECs, or might not be able to effectively facilitate restoring, maintaining or managing CD8$^+$ T cells efficacy to deplete PD-L1$^+$ CTECs, thus accelerating tumor progression in carcinoma patients. Recent clinical studies combining anti-angiogenesis (VEGF/VEGFR inhibitors) and immune checkpoint blockade therapy (anti-PD-L1) showed notable therapeutic responses in breast and pancreatic cancer models [25]. Co-detection and *in situ* phenotypic, karyotypic as well as morphological comprehensive characterization of PD-L1$^+$ aneuploid CTCs and CTECs, are expected to assist in more appropriately evaluating the efficacy of the therapy regimen combining anti-angiogenesis and immunotherapy.

The 5-year overall survival rate of late stage hPD-L1$^+$ lung cancer patients receiving checkpoint blockade immunotherapy has reached 29.6% (ASCO, 2019). However, conventional pathological needle biopsy employed to detect hPD-L1 expression may bring a non-negligible false negativity [4]. The present study showed that, in addition to an effective detection of PD-L1$^+$ aneuploid CTCs in hPD-L1$^+$ subjects, SE-iFISH was also able to effectively detect PD-L1$^+$ CTCs in 44.4% of hPD-L1$^-$ patients prior to immunotherapy. It would be meaningful to further investigate in a substantial sample size of carcinoma patients whether and how co-detection of PD-L1$^+$ CTCs and CTECs could help more appropriately select patients suitable for receiving either first-line or second-line immunotherapy.

In summary, the present study first-ever demonstrated clinical impact of PD-L1 expression on aneuploid CTECs. Both CTCs and CTECs expressing either PD-L1 or Vimentin were identified in the immunotherapeutic NSCLC patients. Aneuploid CTCs and CTECs, respectively bearing the symbolic non-synonymous single nucleotide-polymorphism (SNP) in *TP53* gene for CTCs and *CDKN2A* gene for CTECs [15], may have a cross-talk and potentially function as a pair of real time "cellular circulating tumor biomarkers", each possessing distinct clinical significance. Multidisciplinary studies to further elucidate inherent biological properties and the clinical significance of aneuploid CTCs and CTECs in a large cohort of patients with a variety of malignancies are under way, which will lead to a greater comprehension on whether and how those diverse categories of viable aneuploid cells may have a functional interplay in either circulation or the tumor microenvironment, and what their possible effects on tumor progression, seeding and implantation of metastatic cancer cells, as well as response to clinical therapies are. Future extensive investigation of PD-L1$^+$ $_L$CTECs in carcinoma patients subjected to anti-PD-1 or anti-PD-L1 immunotherapy, will shed light on a better understanding of how PD-1 and PD-L1 interact on diverse types of the host cells, and how such interaction impacts on tumor angiogenesis, progression as well as therapy resistance, ultimately improving the efficacy of either immunotherapy alone or the combo regimens in cancer patients.

Declaration of competing interest

i•FISH® and i•Cyto® are the registered trademarks of Cytelligen. Dr. Peter P. Lin is president at Cytelligen. None of authors owns Cytelligen's stock shares. No additional conflict of interest to be disclosed.

Acknowledgements

Enrollment of patients, performing experiments, acquisition and analysis of data were supported by the grants of Beijing Municipal Administration of Hospitals Incubating Program PX2017050 to LZ, Beijing Municipal Science and Technology Commission Z17110-000101703 to TZ, and Z15110-0002115049 to SX. Authors thank Prof. and President Shaofa Xu, Jinjing Tan and staffs at Beijing Chest Hospital, Cytointelligen (China Medical City, Taizhou, Jiangsu, China), and Cytelligen (San Diego, CA, USA) for providing support. Authors also thank Alexander Y. Lin for helping improve the drafted manuscript. All authors have read and approved the submitted manuscript.

References

[1] D.F. Quail, J.A. Joyce, Microenvironmental regulation of tumor progression and metastasis, Nat. Med. 19 (2013) 1423–1437.
[2] T.L. Whiteside, The tumor microenvironment and its role in promoting tumor growth, Oncogene 27 (2008) 5904–5912.
[3] L.S. Walker, D.M. Sansom, The emerging role of CTLA4 as a cell-extrinsic regulator of T cell responses, Nat. Rev. Immunol. 11 (2011) 852–863.
[4] W. Zou, J.D. Wolchok, L. Chen, PD-L1 (B7-H1) and PD-1 pathway blockade for cancer therapy: mechanisms, response biomarkers, and combinations, Sci. Transl. Med. 8 (2016) 328rv324.
[5] H. Dong, S.E. Strome, D.R. Salomao, H. Tamura, F. Hirano, D.B. Flies, P.C. Roche, J. Lu, G. Zhu, K. Tamada, V.A. Lennon, E. Celis, L. Chen, Tumor-associated B7-H1 promotes T-cell apoptosis: a potential mechanism of immune evasion, Nat. Med. 8 (2002) 793–800.
[6] N. Rodig, T. Ryan, J.A. Allen, H. Pang, N. Grabie, T. Chernova, E.A. Greenfield, S.C. Liang, A.H. Sharpe, A.H. Lichtman, G.J. Freeman, Endothelial expression of PD-L1 and PD-L2 down-regulates CD8+ T cell activation and cytolysis, Eur. J. Immunol. 33 (2003) 3117–3126.
[7] J.R. Brahmer, S.S. Tykodi, L.Q. Chow, W.J. Hwu, S.L. Topalian, P. Hwu, C.G. Drake, L.H. Camacho, J. Kauh, K. Odunsi, H.C. Pitot, O. Hamid, S. Bhatia, R. Martins, K. Eaton, S. Chen, T.M. Salay, S. Alaparthy, J.F. Grosso, A.J. Korman, S.M. Parker, S. Agrawal, S.M. Goldberg, D.M. Pardoll, A. Gupta, J.M. Wigginton, Safety and activity of anti-PD-L1 antibody in patients with advanced cancer, N. Engl. J. Med. 366 (2012) 2455–2465.
[8] L. Chen, X. Han, Anti-PD-1/PD-L1 therapy of human cancer: past, present, and future, J. Clin. Investig. 125 (2015) 3384–3391.
[9] M. Reck, D. Rodriguez-Abreu, A.G. Robinson, R. Hui, T. Csoszi, A. Fulop, M. Gottfried, N. Peled, A. Tafreshi, S. Cuffe, M. O'Brien, S. Rao, K. Hotta, M.A. Leiby, G.M. Lubiniecki, Y. Shentu, R. Rangwala, J.R. Brahmer, Pembrolizumab versus chemotherapy for PD-L1-positive non-small-cell lung cancer, N. Engl. J. Med. 375 (2016) 1823–1833.
[10] J.M. Taube, R.A. Anders, G.D. Young, H. Xu, R. Sharma, T.L. McMiller, S. Chen, A.P. Klein, D.M. Pardoll, S.L. Topalian, L. Chen, Colocalization of inflammatory response with B7-h1 expression in human melanocytic lesions supports an adaptive resistance mechanism of immune escape, Sci. Transl. Med. 4 (2012) 127ra–137.
[11] Y. Li, X. Zhang, D. Liu, J. Gong, D.D. Wang, S. Li, Z. Peng, X. Wang, P.P. Lin, M. Li, L. Shen, Evolutionary expression of HER2 conferred by chromosome aneuploidy on

circulating gastric cancer cells contributes to developing targeted and chemotherapeutic resistance, Clin. Cancer Res. 24 (2018) 5261–5271.
[12] M. Cristofanilli, G.T. Budd, M.J. Ellis, A. Stopeck, J. Matera, M.C. Miller, J.M. Reuben, G.V. Doyle, W.J. Allard, L.W. Terstappen, D.F. Hayes, Circulating tumor cells, disease progression, and survival in metastatic breast cancer, N. Engl. J. Med. 351 (2004) 781–791.
[13] X. Liu, J. Li, B.L. Cadilha, A. Markota, C. Voigt, Z. Huang, P.P. Lin, D.D. Wang, J. Dai, G. Kranz, A. Krandick, D. Libl, H. Zitzelsberger, I. Zagorski, H. Braselmann, M. Pan, S. Zhu, Y. Huang, S. Niedermeyer, C.A. Reichel, B. Uhl, D. Briukhovetska, J. Suarez, S. Kobold, O. Gires, H. Wang, Epithelial-type systemic breast carcinoma cells with a restricted mesenchymal transition are a major source of metastasis, Sci. Adv. 5 (2019) eaav4275.
[14] H. Wang, N.H. Stoecklein, P.P. Lin, O. Gires, Circulating and disseminated tumor cells: diagnostic tools and therapeutic targets in motion, Oncotarget 8 (2017) 1884–1912.
[15] P.P. Lin, Aneuploid CTC and CEC, Diagnostics 8 (2018) 26 (Basel).
[16] P.P. Lin, O. Gires, D.D. Wang, L. Li, H. Wang, Comprehensive *in situ* co-detection of aneuploid circulating endothelial and tumor cells, Sci. Rep. 7 (2017) 9789.
[17] T. Akino, K. Hida, Y. Hida, K. Tsuchiya, D. Freedman, C. Muraki, N. Ohga, K. Matsuda, K. Akiyama, T. Harabayashi, N. Shinohara, K. Nonomura, M. Klagsbrun, M. Shindoh, Cytogenetic abnormalities of tumor-associated endothelial cells in human malignant tumors, Am. J. Pathol. 175 (2009) 2657–2667.
[18] K. Hida, M. Klagsbrun, A new perspective on tumor endothelial cells: unexpected chromosome and centrosome abnormalities, Cancer Res. 65 (2005) 2507–2510.
[19] A.C. Dudley, Tumor endothelial cells, Cold Spring Harb. Perspect. Med. 2 (2012) a006536.
[20] K. Hida, N. Maishi, D.A. Annan, Y. Hida, Contribution of tumor endothelial cells in cancer progression, Int. J. Mol. Sci. 19 (2018) 1272.
[21] F. Bertolini, Y. Shaked, P. Mancuso, R.S. Kerbel, The multifaceted circulating endothelial cell in cancer: towards marker and target identification, Nat. Rev. Cancer 6 (2006) 835–845.
[22] I. Cima, S.L. Kong, D. Sengupta, I.B. Tan, W.M. Phyo, D. Lee, M. Hu, C. Iliescu, I. Alexander, W.L. Goh, M. Rahmani, N.A. Suhaimi, J.H. Vo, J.A. Tai, J.H. Tan, C. Chua, R. Ten, W.J. Lim, M.H. Chew, C.A. Hauser, R.M. van Dam, W.Y. Lim, S. Prabhakar, B. Lim, P.K. Koh, P. Robson, J.Y. Ying, A.M. Hillmer, M.H. Tan, Tumor-derived circulating endothelial cell clusters in colorectal cancer, Sci. Transl. Med. 8 (2016) 345ra–389.
[23] Y. Zhao, J. Li, D. Li, Z. Wang, J. Zhao, X. Wu, Q. Sun, P.P. Lin, P. Plum, A. Damanakis, F. Gebauer, M. Zhou, Z. Zhang, H. Schlosser, K.-W. Jauch, P.J. Nelson, C.J. Bruns, Tumor biology and multidisciplinary strategies of oligometastasis in gastrointestinal cancers, Semin. Cancer Biol. (2019) in press, https://doi.org/10.1016/j.semcancer.2019.08.26.
[24] M. Mazel, W. Jacot, K. Pantel, K. Bartkowiak, D. Topart, L. Cayrefourcq, D. Rossille, T. Maudelonde, T. Fest, C. Alix-Panabieres, Frequent expression of PD-L1 on circulating breast cancer cells, Mol. Oncol. 9 (2015) 1773–1782.
[25] E. Allen, A. Jabouille, L.B. Rivera, I. Lodewijckx, R. Missiaen, V. Steri, K. Feyen, J. Tawney, D. Hanahan, I.P. Michael, G. Bergers, Combined antiangiogenic and anti-PD-L1 therapy stimulates tumor immunity through HEV formation, Sci. Transl. Med. 9 (2017) eaaj9679.
[26] L.F. Campesato, T. Merghoub, Antiangiogenic therapy and immune checkpoint blockade go hand in hand, Ann. Transl. Med. 5 (2017) 497.
[27] M. Kowanetz, W. Zou, S.N. Gettinger, H. Koeppen, M. Kockx, P. Schmid, E.E. Kadel 3rd, I. Wistuba, J. Chaft, N.A. Rizvi, D.R. Spigel, A. Spira, F.R. Hirsch, V. Cohen, D. Smith, Z. Boyd, N. Miley, S. Flynn, V. Leveque, D.S. Shames, M. Ballinger, S. Mocci, G. Shankar, R. Funke, G. Hampton, A. Sandler, L. Amler, I. Mellman, D.S. Chen, P.S. Hegde, Differential regulation of PD-L1 expression by immune and tumor cells in NSCLC and the response to treatment with atezolizumab (anti-PD-L1), Proc. Natl. Acad. Sci. U.S.A. 115 (2018) E10119–E10126.
[28] N. Guibert, M. Delaunay, A. Lusque, N. Boubekeur, I. Rouquette, E. Clermont, J. Mourlanette, S. Gouin, I. Dormoy, G. Favre, J. Mazieres, A. Pradines, PD-L1 expression in circulating tumor cells of advanced non-small cell lung cancer patients treated with nivolumab, Lung Cancer 120 (2018) 108–112.
[29] M. Ilie, E. Szafer-Glusman, V. Hofman, E. Chamorey, S. Lalvee, E. Selva, S. Leroy, C.H. Marquette, M. Kowanetz, P. Hedge, E. Punnoose, P. Hofman, Detection of PD-L1 in circulating tumor cells and white blood cells from patients with advanced non-small-cell lung cancer, Ann. Oncol. 29 (2018) 193–199.
[30] G. Kallergi, E.K. Vetsika, D. Aggouraki, E. Lagoudaki, A. Koutsopoulos, F. Koinis, P. Katsarlinos, M. Trypaki, I. Messaritakis, C. Stournaras, V. Georgoulias, A. Kotsakis, Evaluation of PD-L1/PD-1 on circulating tumor cells in patients with advanced non-small cell lung cancer, Ther. Adv. Med. Oncol. 10 (2018) 1758834017750121.
[31] A. Satelli, I.S. Batth, Z. Brownlee, C. Rojas, Q.H. Meng, S. Kopetz, S. Li, Potential role of nuclear PD-L1 expression in cell-surface vimentin positive circulating tumor cells as a prognostic marker in cancer patients, Sci. Rep. 6 (2016) 28910.
[32] C. Yue, Y. Jiang, P. Li, Y. Wang, J. Xue, N. Li, D. Li, R. Wang, Y. Dang, Z. Hu, Y. Yang, J. Xu, Dynamic change of PD-L1 expression on circulating tumor cells in advanced solid tumor patients undergoing PD-1 blockade therapy, OncoImmunology 7 (2018) e1438111.
[33] L. Wang, Y. Li, J. Xu, A. Zhang, X. Wang, R. Tang, X. Zhang, H. Yin, M. Liu, D.D. Wang, P.P. Lin, L. Shen, J. Dong, Quantified postsurgical small cell size CTCs and EpCAM^{+} circulating tumor stem cells with cytogenetic abnormalities in hepatocellular carcinoma patients determine cancer relapse, Cancer Lett. 412 (2018) 99–107.
[34] P.P. Lin, Integrated EpCAM-independent subtraction enrichment and iFISH strategies to detect and classify disseminated and circulating tumors cells, Clin. Transl. Med. 4 (2015) 38.
[35] P. Lin, T. Fischer, T. Weiss, M.G. Farquhar, Calnuc, an EF-hand Ca^{2+} binding protein, specifically interacts with the C-terminal α5-helix of Gαi3, Proc. Natl. Acad. Sci. U.S.A. 97 (2000) 674–679.
[36] P. Lin, T. Fischer, C. Lavoie, H. Huang, M.G. Farquhar, Calnuc plays a role in dynamic distribution of Gαi but not Gβ subunits and modulates ACTH secretion in AtT-20 neuroendocrine secretory cells, Mol. Neurodegener. 4 (2009) 1–15.
[37] J. Zhou, K.M. Mahoney, A. Giobbie-Hurder, F. Zhao, S. Lee, X. Liao, S. Rodig, J. Li, X. Wu, L.H. Butterfield, M. Piesche, M.P. Manos, L.M. Eastman, G. Dranoff, G.J. Freeman, F.S. Hodi, Soluble PD-L1 as a biomarker in malignant melanoma treated with checkpoint blockade, Cancer Immunol. Res. 5 (2017) 480–492.
[38] O. Gires, N.H. Stoecklein, Dynamic EpCAM expression on circulating and disseminating tumor cells: causes and consequences, Cell. Mol. Life Sci.: CMLS 71 (2014) 4393–4402.
[39] U. Kronenwett, S. Huwendiek, C. Ostring, N. Portwood, U.J. Roblick, Y. Pawitan, A. Alaiya, R. Sennerstam, A. Zetterberg, G. Auer, Improved grading of breast adenocarcinomas based on genomic instability, Cancer Res. 64 (2004) 904–909.
[40] Y.L. Li, X.T. Zhang, S. Ge, J. Gao, J.F. Gong, M. Lu, Q.Y. Zhang, Y.S. Cao, D.D. Wang, P.P. Lin, L. Shen, Clinical significance of phenotyping and karyotyping of circulating tumor cells in patients with advanced gastric cancer, Oncotarget 5 (2014) 6594–6602.
[41] D.J. Gordon, B. Resio, D. Pellman, Causes and consequences of aneuploidy in cancer, Nat. Rev. Genet. 13 (2012) 189–203.
[42] G.J. Kops, B.A. Weaver, D.W. Cleveland, On the road to cancer: aneuploidy and the mitotic checkpoint, Nat. Rev. Cancer 5 (2005) 773–785.
[43] M. Durrbaum, Z. Storchova, Effects of aneuploidy on gene expression: implications for cancer, FEBS J. 283 (2016) 791–802.
[44] L. Sansregret, C. Swanton, The role of aneuploidy in cancer evolution, Cold Spring Harb. Perspect. Med. 7 (2017) a028373.
[45] J. Jiang, D.D. Wang, M. Yang, D. Chen, L. Pang, S. Guo, J. Cai, J.P. Wery, L. Li, H. Li, P.P. Lin, Comprehensive characterization of chemotherapeutic efficacy on metastases in the established gastric neuroendocrine cancer patient derived xenograft model, Oncotarget 6 (2015) 15639–15651.
[46] S. Piera-Velazquez, F.A. Mendoza, S.A. Jimenez, Endothelial to mesenchymal transition (EndoMT) in the pathogenesis of human fibrotic diseases, J. Clin. Med. 5 (2016) 45.
[47] A. Satelli, S. Li, Vimentin in cancer and its potential as a molecular target for cancer therapy, Cell. Mol. Life Sci.: CMLS 68 (2011) 3033–3046.
[48] M. Yu, A. Bardia, B.S. Wittner, S.L. Stott, M.E. Smas, D.T. Ting, S.J. Isakoff, J.C. Ciciliano, M.N. Wells, A.M. Shah, K.F. Concannon, M.C. Donaldson, L.V. Sequist, E. Brachtel, D. Sgroi, J. Baselga, S. Ramaswamy, M. Toner, D.A. Haber, S. Maheswaran, Circulating breast tumor cells exhibit dynamic changes in epithelial and mesenchymal composition, Science 339 (2013) 580–584.
[49] Y. Manjunath, S.V. Upparahalli, D.M. Avella, C.B. Deroche, E.T. Kimchi, K.F. Staveley-O'Carroll, C.J. Smith, G. Li, J.T. Kaifi, PD-L1 expression with epithelial mesenchymal transition of circulating tumor cells is associated with poor survival in curatively resected non-small cell lung cancer, Cancers (Basel) 11 (2019) 806.
[50] A.K. Thar Min, H. Okayama, M. Saito, M. Ashizawa, K. Aoto, T. Nakajima, K. Saito, S. Hayase, W. Sakamoto, T. Tada, H. Hanayama, Z. Saze, T. Momma, S. Ohki, Y. Sato, S. Motoyama, K. Mimura, K. Kono, Epithelial-mesenchymal transition-converted tumor cells can induce T-cell apoptosis through upregulation of programmed death ligand 1 expression in esophageal squamous cell carcinoma, Cancer Med 7 (2018) 3321–3330.
[51] H. Ghebeh, C. Lehe, E. Barhoush, K. Al-Romaih, A. Tulbah, M. Al-Alwan, S.F. Hendrayani, P. Manogaran, A. Alaiya, T. Al-Tweigeri, A. Aboussekhra, S. Dermime, Doxorubicin downregulates cell surface B7-H1 expression and upregulates its nuclear expression in breast cancer cells: role of B7-H1 as an anti-apoptotic molecule, Breast Cancer Res. 12 (2010) R48.
[52] E. Lanitis, D. Dangaj, M. Irving, G. Coukos, Mechanisms regulating T-cell infiltration and activity in solid tumors, Ann. Oncol. 28 (2017) xii18–xii32.